Mössbauer and X-ray Diffraction Studies of Cubic Solid Solutions of the $ZrO_2-Y_2O_3-Fe_2O_3$ System

A. G. Belous,[†] E. V. Pashkova,[†] K. V. Kravchyk,*[,†] V. P. Ivanitskii,[‡] and O. I. V'yunov[†]

V. I. Vernadskii Institute of General and Inorganic Chemistry, Palladina Avenue 32/34 03680, Kyiv-142, Ukraine, and Institute of Geochemistry, Mineralogy and Ore Formation, Palladina Avenue 34, 03680 Kyiv-142, Ukraine

Received: October 22, 2007; In Final Form: December 17, 2007

The effect of iron oxide on the polymorphic composition and thin structure of cubic solid solutions of the $(ZrO_2)_{0.9}(Y_2O_3)_{0.1-x}(Fe_2O_3)_x$ system has been investigated. The maximum Fe_2O_3 solubility in the studied cut of the ternary system has been determined to be 2 mol %. Iron exists only as Fe^{3+} ions in octahedral coordination. Three nonequivalent positions of the Fe^{3+} ions, which differ in surrounding cations and anions, have been identified. It has been shown that Fe_2O_3 is not a stabilizer of the high-temperature modifications of ZrO_2, but it promotes the stabilizing action (efficiency) of Y_2O_3 and structure stability in time due to the formation of the compound $YFeO_3$ with structure isomorphic to *c*-ZrO_2.

Introduction

The $ZrO_2-Y_2O_3-Fe_2O_3$ system is of great practical importance because it can be used for developing solid electrolytes with oxygen conductivity.[1−3] The decrease of average cation radius in the case of partial substitution of Y^{3+} ions by smaller Fe^{3+} ions (for coordination number 6, $rY^{3+} = 0.892$ Å, $rFe^{3+} = 0.645$ Å[4]) usually improves the conditions for transport of O^{2-} ions.[5,6] Moreover, the sintering temperature of ceramics considerably decreases.[7−8]

One of the problems in development of solid electrolytes based on ZrO_2 is the preparation of fully stabilized (without monoclinic (m) phase) zirconium dioxide with cubic (c) unit cell of fluorite type (CaF_2), which would ensure the stability of electrophysical properties. This phase must be stable against external actions: temperature, pressure, and various gas and liquid media.[9] Today, the absence of a clear picture of the mechanism of stabilization and destabilization of high-temperature ZrO_2 modifications prevents the successful solution of the above problem. Therefore, the investigation of polymorphism and structure features of the systems based on ZrO_2 depending on the conditions of heat treatment and chemical composition is topical.

The presented work is a continuation of our previous investigations.[10] In ref 10, the polymorphic composition in the system $[1-(x+y)]ZrO_2{\cdot}xY_2O_3{\cdot}yFe_2O_3$ for compositions with $x + y = 0.03-0.08$ has been investigated as a function of the chemical composition and heat treatment conditions, and the fine structure of tetragonal (t) solid solutions has also been studied using Mössbauer spectroscopy. At high temperatures, both ion conductivity and activation energy are higher for cubic solid solution (SS) than for tetragonal SS.[11] Therefore, the investigation of the fine structure of *c*-ZrO_2-based SS is of interest. In the binary $ZrO_2-Y_2O_3$ system, *c*-ZrO_2 is fully stabilized for a Y_2O_3 content of 8−9 mol %.[12] In the $ZrO_2-Y_2O_3-Fe_2O_3$ system, *c*-ZrO_2 and *t*-ZrO_2 are fully stabilized for a total Y_2O_3 and Fe_2O_3 content of 8 mol %.[10] Taking into account these results, it is possible to expect crystallization of single-phase *c*-ZrO_2 for a total Y_2O_3 and Fe_2O_3 content of 10−12 mol %.

The aim of this work is to investigate the structure features of cubic solid solutions of the $(ZrO_2)_{0.9}(Y_2O_3)_{0.1-x}(Fe_2O_3)_x$ system.

Experimental Methods

Samples of complex oxides of $(ZrO_2)_{0.9}(Y_2O_3)_{0.1-x}(Fe_2O_3)_x$ compositions with $x = 0$, 0.01, 0.015, 0.02, 0.03, 0.04, and 0.05 were investigated. Oxides were prepared by calcining $ZrO(OH)_2$, $Y(OH)_3$, and FeOOH hydroxides, precipitated from concentrated solutions of $ZrOCl_2$, $Y(NO)_3$, and $Fe(NO)_3$ with an ammonia solution. Precipitation was carried out in two stages: at first, $ZrO(OH)_2$ and FeOOH were coprecipitated, and then $Y(OH)_3$ was precipitated. The precipitates were washed to remove Cl^- and NO_3^- ions and dried at 350 K. Heat treatment was performed in a chamber furnace at 1220−1620 K.

Chemical compositions were determined for samples after heat treatment at 1470 and 1620 K. Iron content was determined using an atomic-absorption spectrometer SP9, Pye Unicom ($\lambda = 248.3$ nm, slit width 0.2 nm, acetone/air flame). Zirconium and yttrium content was determined as described in ref 13.

X-ray phase and full-profile analyses were carried out using a DRON-4−07 diffractometer (Cu Kα radiation, step-scan mode with a step size of 0.02° and a counting time per data point of 10 s). SiO_2 (2Θ standard) and NIST SRM 1976 − Al_2O_3 (certified intensity standard[14]) were used as external standards. The samples were investigated just after heat treatment and after storing them in air for 2 years. PDF database was used for phase analysis. X-ray integral peaks intensity of corresponding phases and equations from ref 10 were used for quantitative analysis of percentage of different ZrO_2 polymorphic modifications and α-Fe_2O_3 (the measurement error was 5%). Structure parameters were adjusted by Rietveld full-profile analysis using FullProf software.

* To whom correspondence should be addressed. Tel/Fax: +380-44-4242211. E-mail: krawtschyk@yahoo.com.
[†] V. I. Vernadskii Institute of General and Inorganic Chemistry.
[‡] Institute of Geochemistry.

10.1021/jp7102148 CCC: $40.75
Published on Web 02/19/2008 PAGE EST: 5.9

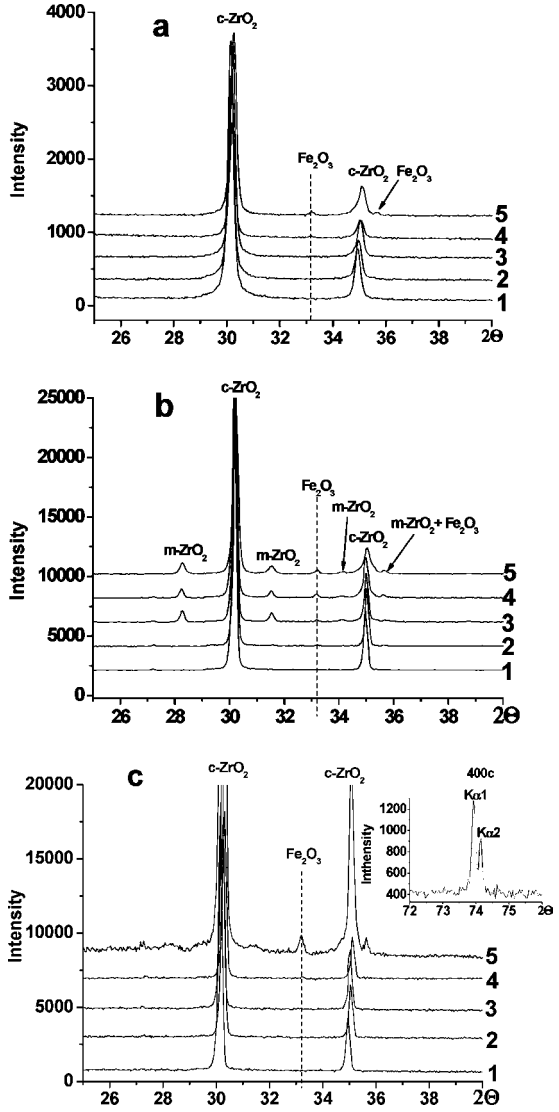

Figure 1. X-ray patterns of $(ZrO_2)_{0.9}(Y_2O_3)_{0.1-x}(Fe_2O_3)_x$ samples after heat treatment at 1223 (a), 1473 (b), and 1623 K (c); $x = 0.01$ (1), 0.02 (2), 0.03 (3), 0.04 (4), and 0.05 (5).

Mössbauer spectra (MS) were obtained by using an electrodynamic spectrometer which operates in the constant-acceleration mode with a 57Co γ-quantum source in Rh matrix. The measurements were made at room temperature. The calibrations of the velocity scale in the magnetic and paramagnetic measurement ranges were performed by means of α-Fe and sodium nitroprusside respectively (to reduce the isomer shift values, given relative to α-Fe, to isomer shifts relative to sodium nitroprusside, 0.258 mm/s must be added to the first value). The isomer shifts for the spectra of each of the ranges (V) were given with respect to the calibrations used. The spectra were processed using a program that realizes the least-squares method.

Results and Discussion

Figure 1 shows X-ray powder diffraction (XRPD) patterns of samples of the $(ZrO_2)_{0.9}(Y_2O_3)_{0.1-x}(Fe_2O_3)_x$ system ($x = 0.01$, 0.02, 0.03, 0.04, and 0.05) after heat treatment at 1223, 1473, and 1623 K, and Table 1 lists phase compositions of these samples. The main phase at these temperatures is cubic zirconium dioxide (c-ZrO_2) with fluorite structure. Tetragonal phase (t-ZrO_2) is absent. Peak 400 of c-ZrO_2 at $2\Theta = 73-74°$ (inset in Figure 1) split only into Ka_1 and Ka_2 constituents.[15] In the temperature range 1223−1573 K, samples are cubic and single-phase ones at $x = 0-0.02$. With increase of x above 0.03 and/or T above 1223 K, additional α-Fe_2O_3 and m-ZrO_2 phases appear (Figure 1, Table 1).

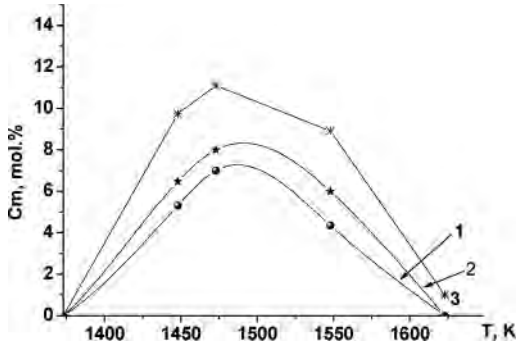

Figure 2. Temperature dependence of the monoclinic phase content of $(ZrO_2)_{0.9}(Y_2O_3)_{0.1-x}(Fe_2O_3)_x$ samples at different Fe_2O_3 content; $x =$ 0.03 (1), 0.04 (2), and 0.05 (3).

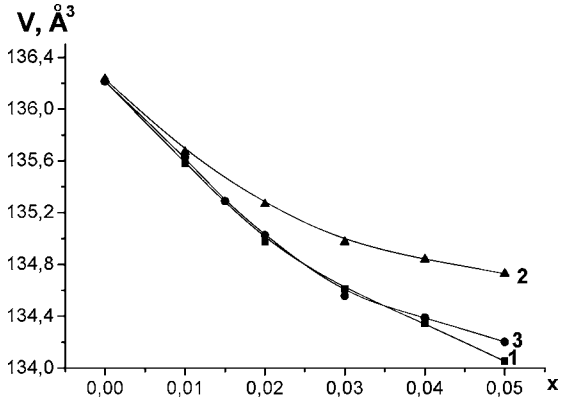

Figure 3. Concentration dependence of unit cell parameters of $(ZrO_2)_{0.9}(Y_2O_3)_{0.1-x}(Fe_2O_3)_x$ samples at different temperatures: 1223 (1), 1473 (2), and 1623 K (3).

Figure 2 shows temperature dependences of m-ZrO_2 phase content for samples with $x = 0.03-0.05$. ZrO_2 is destabilized at 1373−1473 K (the amount of m-ZrO_2 phase increases) and stabilized at temperatures above 1473 K.

The x dependences of unit cell parameter of c-ZrO_2 in x regions 0−0.02 and 0.03−0.05 after heat treatment at 1223, 1473, and 1623 K obey Vegard rule (Figure 3). This indicates that substitutional SS are formed. At $x > 0.02$, an inflection of $a-x$ curve is observed due to formation of multiphase material (c-ZrO_2, m-ZrO_2, and α-Fe_2O_3, see Table 1) and, consequently, due to the decrease of Fe_2O_3 solubility in c-ZrO_2 in the region $x > 0.02-0.05$. XRPD data (Table 1) show the Fe_2O_3 solubility limit for the investigated system to be 2 mol % at 1473 K and 3 mol % at 1673 K. To specify the mechanism and to refine the limit of Fe_2O_3 solubility in ZrO_2, Mössbauer spectra of samples $(ZrO_2)_{0.9}(Y_2O_3)_{0.08}(Fe_2O_3)_{0.02}$ (I) and $(ZrO_2)_{0.9}(Y_2O_3)_{0.07}$-$(Fe_2O_3)_{0.03}$ (II) after heat treatment at 1473 and 1623 K (samples I, II and I′, II′, respectively) were analyzed. The results of a chemical analysis of these samples (Table 2) support the correspondence of the actual composition to the predetermined one (within the error of analysis).

The MSs obtained in the magnetic range are shown in Figure 4, and their parameters are listed in Table 3. The spectrum of sample I is represented by a superposition of a magnetic splitting sextet and a high-intensity broadened quadrupole splitting doublet with equal intensities and widths of absorption lines.

TABLE 1: Phase Composition of $(ZrO_2)_{0.9}(Y_2O_3)_{0.1-x}(Fe_2O_3)_x$ Samples as a Function of the Chemical Composition (x) and Heat Treatment Temperature

no.	heat treatment temperature, K	$x = 0.01$	$x = 0.02$	$x = 0.03$	$x = 0.04$	$x = 0.05$
1	1223	*c*-ZrO_2 (100)[a]	*c*-ZrO_2 (100)	*c*-ZrO_2 (100)	*c*-ZrO_2 (99) α-Fe_2O_3 (1)	*c*-ZrO_2 (97.7) α-Fe_2O_3 (2.3)
2	1373	*c*-ZrO_2 (100)	*c*-ZrO_2 (100)	*c*-ZrO_2 (98.7) α-Fe_2O_3 (1.3)	*c*-ZrO_2 (98.2) α-Fe_2O_3 (1.8)	*c*-ZrO_2 (94.7) *m*-ZrO_2 (3.7) α-Fe_2O_3 (1.6)
3	1473	*c*-ZrO_2 (100)	*c*-ZrO_2 (100)	*c*-ZrO_2 (88) *m*-ZrO_2 (10.3) α-Fe_2O_3 (1.7)	*c*-ZrO_2 (89) *m*-ZrO_2 (8.3) α-Fe_2O_3 (2.7)	*c*-ZrO_2 (83) *m*-ZrO_2 (14) α-Fe_2O_3 (3)
4	1673	*c*-ZrO_2 (100)	*c*-ZrO_2 (100)	*c*-ZrO_2 (100)	*c*-ZrO_2 (98) α-Fe_2O_3 (2)	*c*-ZrO_2 (94) *m*-ZrO_2 (4) α-Fe_2O_3 (2)

[a] In brackets is given the quantitative composition of phases (%) calculated from the integral intensity of X-ray peaks.

TABLE 2: Results of a Chemical Analysis of $(ZrO_2)_{0.9}(Y_2O_3)_{0.08}(Fe_2O_3)_{0.02}$ and $(ZrO_2)_{0.9}(Y_2O_3)_{0.07}(Fe_2O_3)_{0.03}$ Samples after Heat Treatment at 1473 and 1623 K

	composition, wt. %			
	$(ZrO_2)_{0.9}(Y_2O_3)_{0.08}-(Fe_2O_3)_{0.02}$(I)		$(ZrO_2)_{0.9}(Y_2O_3)_{0.07}-(Fe_2O_3)_{0.03}$(II)	
oxide analyzed	predetermined	actual	predetermined	actual
ZrO_2	83.9	83.8[a] 84.0	84.35	84.4[a] 84.3
Y_2O_3	13.7	13.7 13.6	12.0	12.0 12.0
Fe_2O_3	2.4	2.6 2.45	3.65	3.5 3.7

[a] The actual compositions of samples after heat treatment at 1473 and 1623 K are given in the first and second line respectively.

The spectrum of sample II is represented by a superposition of two Zeeman splitting sextets and a quadrupole splitting doublet. The MS of sample I′ is represented by a broadened quadrupole splitting doublet, and the MS of sample II′ is represented by a superposition of a similar doublet and a magnetic splitting sextet. The sextets with $H_{eff} = 510-514$ kOe and $H_{eff} = 493$ kOe are associated with the resonance absorption of Fe^{3+} ions in gematite (α-Fe_2O_3) and orthoferrite ($YFeO_3$) structures, respectively, since these parameters (see Figure 4 and Table 3) are close to the published data for iron oxides[16,17] and compounds of the Fe−Y−O system.[18] Because MS lines are broad and have no visible separate components (Figure 4), we tried a mathematical approach to separate the lines of slightly resolved spectra.[19] This approach allows one to find unresolved lines in experimental spectra using their narrowing and to fit experimental data using a hypothesis model. By applying this approach to experimental spectra of samples I and II, two doublets with close values of isomer shift (IS) and different values of quadrupole splitting (QS) were discerned. Using data for isomer shift and quadrupole splitting of ions with different valence and coordination,[20] the discerned doublets were attributed by us to the resonance absorption of gamma-quanta on the high-spin octahedrally coordinated nucleus of Fe^{3+} ions. Eight-coordinated positions, which are characteristic of host Zr^{4+}, are not suitable for Fe^{3+} not only due to the fact that the ionic radius of Fe^{3+} is smaller than that of Zr^{4+} and Y^{3+} (for coordination number 6, $rFe^{3+}_{HS} = 0.645$ Å, $rZr^{4+} = 0.72$ Å, $rY^{3+} = 0.892$ Å; for coordination number 8, $rZr^{4+} = 0.84$ Å, $rY^{3+} = 1.015$ Å[4]) but also due to electroneutrality requirements to crystal lattice. In the case of substitution $2Zr^{4+} \rightarrow 2Y^{3+}$ or $2Zr^{4+} \rightarrow 2Fe^{3+}$ or $2Zr^{4+} \rightarrow Y^{3+} + Fe^{3+}$, negative charge is neutralized by release of O^{2-} from anion polyhedron.[21] The decrease in interatomic distances in the oxygen polyhedron on the partial substitution of Fe^{3+} for Y^{3+} ions enhances the electrostatic repulsion of oxygen ions,[22] which facilitates the formation of octahedral coordination of Fe^{3+} ions. The parameters of paramagnetic doublets are close to the values in ref 23, in which such a doublet is associated with the Fe^{3+} ions dissolved in ZrO_2.

Two MS doublets for samples I and II (Figure 4) are observed due to possible presence of a few iron-containing phases or a few structurally nonequivalent positions of Fe^{3+} ions, which differ in cationic and anionic environment. The analysis of MS parameters (Table 3) and phase contents (Figure 1, Table 1) shows that paramagnetic Fe_1^{3+} and Fe_2^{3+} doublets relate to iron in different ZrO_2 modifications. After heat treatment at 1473 K, the sample with 3 mol % Fe_2O_3 ($x = 0.03$) contains two ZrO_2 modifications (*c*-ZrO_2 and *m*-ZrO_2), but after heat treatment at 1623 K, the sample is single-phase *c*-ZrO_2 (see Table 1). Analysis of MS shows that Fe_2^{3+} and Fe_1^{3+} doublets relate to the above ZrO_2 modifications respectively (Table 3, samples II and II′). For the sample with 2 mol % Fe_2O_3 ($x = 0.02$), a similar assignment is evidently valid since the parameters of MS doublets of samples I, II and I′, II′ are close together (Table 3). In sample I ($x = 0.02$), in contrast to sample II ($x = 0.03$), XRPD shows no *m*-ZrO_2 phase (Figure 1, Table 1) probably due to its low content or noncrystalline state, resulting from small particle size and structure imperfection. The higher values of QS and fwhm (full width at half maxima of MS line) support this statement (see Table 3). The $YFeO_3$ phase is not observed in sample II probably due to its small amount (Figure 1).

To find the unresolved components of broadened doublets, MSs were obtained in the paramagnetic range. Figure 5 shows spectra of samples I′ and II′ after heat treatment at 1623 K. The procedure for the mathematical separation of lines, which are a superposition of several components, which are less than fwhm value apart (as MS lines of samples I′ and II′), is incorrect, as shown in ref 24, which excludes their unambiguous interpretation. In such a case, the data obtained may be considered as valid if they have a physical meaning and correlation parameters have satisfactory values. To fit experimental data by doublet model and to find unresolved MS lines, we used mathematical methods of narrowing lines[19] (Figure 6) and analyzing isomer shift distribution functions (DISTRI program).[25] MSs were found to have to be divided into three doublets of different intensity. Figure 5 shows the results of such division using least-squares method. Parameters of MS doublets are listed in Table 4. The experimental MS of sample I′ (Figure 5a) consists of three quadruple splitting doublets, which have close IS values and significantly different QS values. The parameters of all doublets are characteristic of high-spin

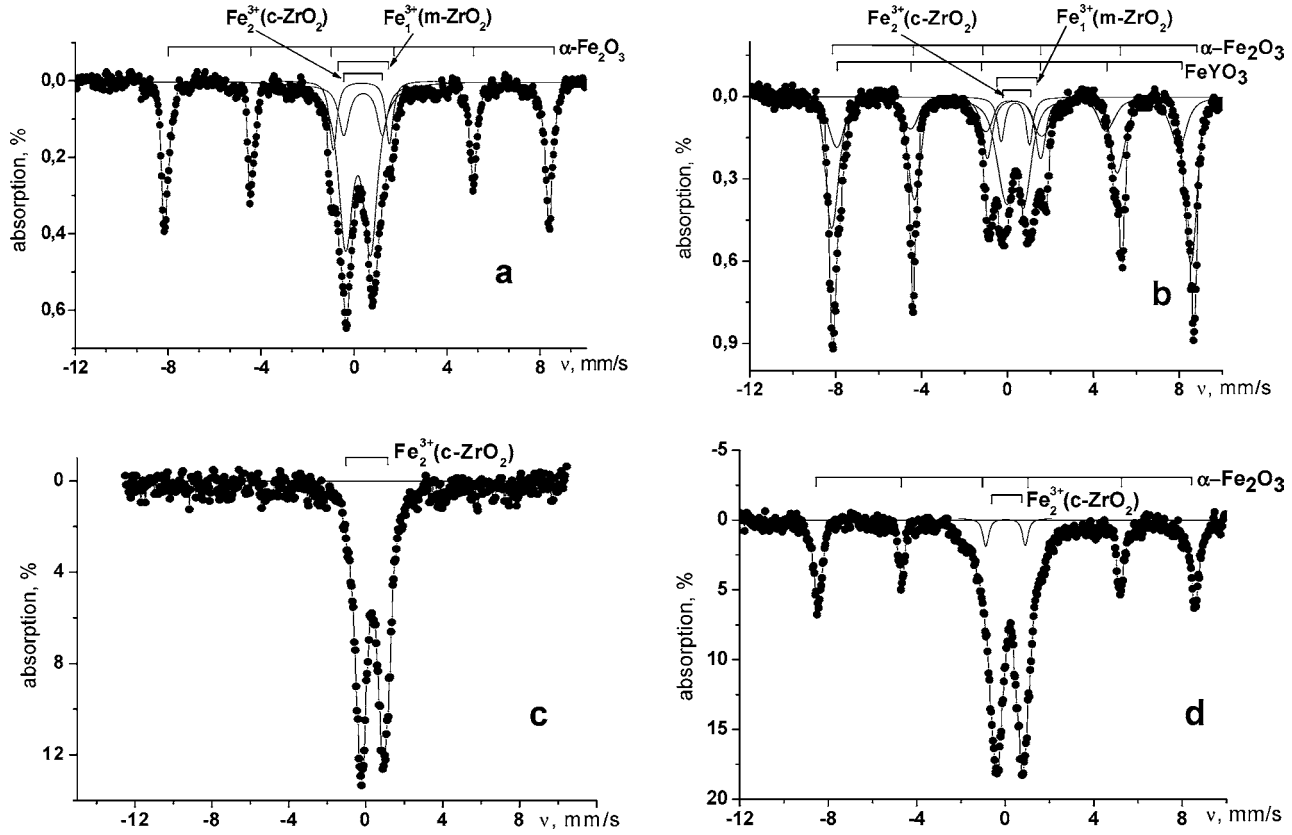

Figure 4. Mössbauer spectra of samples I (a), II (b), I′ (c), and II′ (d) in the magnetic measuring range.

TABLE 3: MS Parameters in the Magnetic Range of $(ZrO_2)_{0.9}(Y_2O_3)_{0.08}(Fe_2O_3)_{0.02}$ (I) and $(ZrO_2)_{0.9}(Y_2O_3)_{0.07}(Fe_2O_3)_{0.03}$ (II) Samples after Heat Treatment at Different Temperatures[a]

sample	temp, K	ion, phase	H_{eff}, kOe	IS, mm/s	QS, mm/s	fwhm, mm/s	S, %
I	1473	α-Fe_2O_3	510	0.64	0.21	0.27	39.2
		Fe_1^{3+} (*m*-ZrO_2)	0	0.70	1.77	0.55	10.2
		Fe_2^{3+} (*c*-ZrO_2)	0	0.63	1.10	0.63	50.6
I′	1623	Fe^{3+} (*c*-ZrO_2)	0	0.60	1.17	0.65	100.0
II	1473	α-Fe_2O_3	514	0.64	0.21	0.31	45.0
		$YFeO_3$	493	0.53	0.04	0.45	27.6
		Fe_1^{3+} (*m*-ZrO_2)	0	0.66	1.58	0.38	5.6
		Fe_2^{3+} (*c*-ZrO_2)	0	0.65	0.97	0.63	21.8
II′	1623	α-Fe_2O_3	510	0.61	0.2	0.36	29.0
		Fe^{3+} (*c*-ZrO_2)	0	0.63	1.18	0.67	71.0

[a] H_{eff} = effective magnetic field; IS = isomer shift relative to sodium nitroprusside, QS = quadrupole splitting; fwhm = absorption line full width at half-maxima; S = relative area of component. Measurement error of IS, QS, and fwhm: ±0.04 mm/s, H_{eff}: ±5 kOe, S: ≤10%.

Fe^{3+} ions in octahedral coordination. QS values significantly differ due to different degree of distortion of the coordination environment of Fe^{3+} resonance ions. The increase of distortions of coordination polyhedron causes an increase of gradients of electric fields on nuclei of resonance ions and, therefore, an increase of QS values. The MS of sample II′ (Figure 5) consists of three Fe^{3+} doublets, the parameters of which are close to the values for sample I′ (Table 4). Therefore, the origin of the absorption lines for both samples is the same. Doublet 4 with intensity 5.4% is a part of the sextet (internal third and fourth lines) of Fe^{3+} magnetic splitting in hematite structure. It is known that the ratio of line intensities in the sextet is 3:2:1:1:2:3, and that the area of the third and fourth lines is 1/6 of the total sextet area. If the area of the internal lines is 5.4%, then the total area of the hematite sextet will be 32.4% (6 times more), which is close to the value measured in the magnetic range (see Table 3; 29% α-Fe_2O_3 in sample II′). Namely, the ratios of Fe^{3+} concentrations in magnetic and paramagnetic phases for different measurements are the same within the experimental errors. The total sextet areas (S_0) calculated are listed in Table 4.

XRPD (Table 1) and analysis of MSs in the magnetic range (Table 3, samples I′ and II′) show that in ZrO_2-based solid solution, a paramagnetic phase consists of *c*-ZrO_2 phase only. Therefore, a few doublets in the paramagnetic range arise from the effect of the cationic environment of Fe^{3+} ions and/or from the presence of regions with preferential localization of Fe^{3+} ions, i.e., with cluster character of iron distribution in ZrO_2-based solid solution. In the binary $ZrO_2-Fe_2O_3$ system, Fe^{3+} clusters were visualized by high-resolution electron microscopy.[26]

Fe^{3+} ions are introduced in both *c*-ZrO_2 and *m*-ZrO_2 (Table 3, sample II). Taking into account the percentage of ZrO_2 polymorphic modifications (Table 1) and the Fe^{3+} content of them (S value in Table 3), it is easy to calculate the Fe^{3+} solubility limit for these modifications. At 1473 K, the Fe^{3+} solubility limit in the *m*-ZrO_2 phase is twice as high as that in the *c*-ZrO_2 phase. Similar results were obtained for the binary system $ZrO_2-Fe_2O_3$.[27] XRPD analysis of samples of this system after heat treatment at 1773 K shows that only m-ZrO_2 phase is observed in samples with Fe_2O_3 content less than 10 mol %, and that additional α-Fe_2O_3 phase is observed in samples with Fe_2O_3 content more than 10 mol %. These and our previous[10] results allow the statement that Fe_2O_3 dissolves only partly in the crystal lattice of ZrO_2 but is not a stabilizer of its high-temperature modifications.

However, in the ternary $ZrO_2-Y_2O_3-Fe_2O_3$ system, Fe_2O_3 facilitates the stabilization of ZrO_2 and increases the efficiency of Y_2O_3 as a stabilizer of high-temperature ZrO_2. The com-

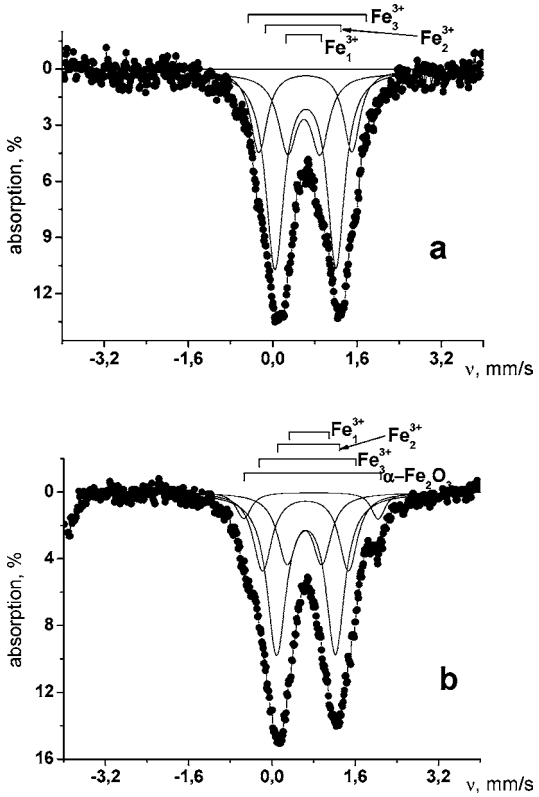

Figure 5. Mössbauer spectra of samples I (a), II (b), I′ (c), and II′ (d) in the paramagnetic measuring range.

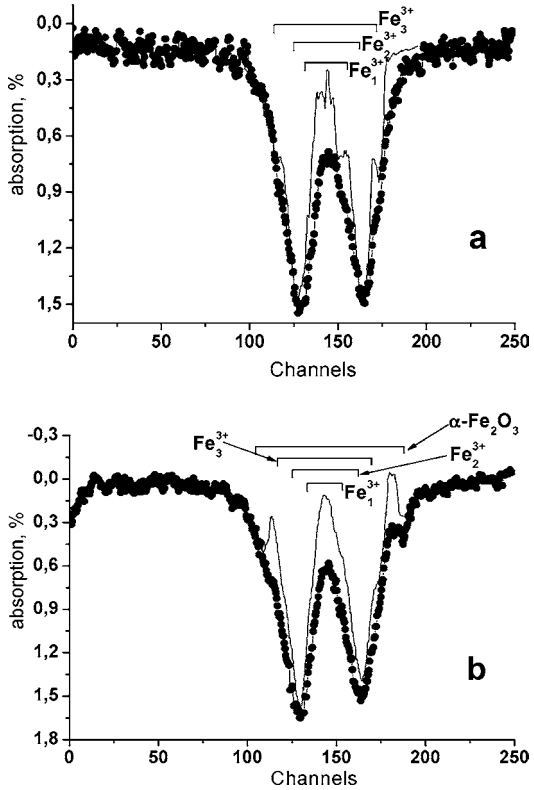

Figure 6. Results of fitting of the Mössbauer spectra of samples I′ (a) and II′ (b) by the method of narrowing lines.

parison of polymorphic transformations during heat treatment of precursors (hydroxides) in the binary $ZrO_2-Y_2O_3$ system[28] and the ternary $ZrO_2-Y_2O_3-Fe_2O_3$[10] system clearly shows this peculiarity. Namely, in the binary system containing 2 mol % Y_2O_3, high-temperature modifications are not stabilized,[28] but in the ternary system containing 2 mol % Y_2O_3 and 2 mol % Fe_2O_3, high-temperature modifications are partially stabilized, and the *m*-ZrO_2 content is no more than 5 mol %.[10] Moreover, Table 1 and results of ref 10 show that Fe_2O_3 facilitates the stabilization of *c*-ZrO_2. Table 4 shows that for sample III, the fraction of paramagnetic component in the total area of the MS of the introduced iron is 70.6%. This indicates that of introduced 3 mol % Fe_2O_3, 2.1 mol % dissolves in *c*-ZrO_2, and 0.9 mol % precipitates as Fe_2O_3. XRPD does not contain the reflects of Fe_2O_3 phase due to its low content (Table 1). Fe_2O_3 solubility limit in the section $(ZrO_2)_{0.9}(Y_2O_3)_{0.1-x}(Fe_2O_3)_x$ for 7 mol % Y_2O_3 is 2 mol %. The increase of Y_2O_3 to 10 mol % increases Fe_2O_3 solubility to 4 mol %.[29] Thus, Fe_2O_3 solubility in the ZrO_2 crystal lattice increases with an increase of Y_2O_3 content. Fe_2O_3 stabilizes ZrO_2 only if Y_2O_3 is added to SS due to the steric factor or to the formation of stabilizing complex oxide of yttrium and iron. The authors of refs 22 and 30 consider that the stabilization of high-temperature ZrO_2 modifications occurs mainly due to the decrease of electrostatic repulsion between oxygen ions as a result of aliovalent substitution of relatively large ions (Y^{3+}, Ca^{2+}, and Ce^{4+}) for smaller Zr^{4+} ions, which is accompanied with an increase of unit cell parameters. However this statement and our results do not agree. Substitution of Fe^{3+} for Y^{3+} decreases the unit cell parameters of ZrO_2-based SS (see Figure 3), but the sample remains single-phase *c*-ZrO_2 (Figure 1, Table 1). The polymorphic state of SS based on $ZrO_2-Y_2O_3$ at room temperature was analyzed by us in terms of steric factor. The data of ref 4 were used for calculation. The following ranges of average cation radii were found for

TABLE 4: MS Parameters in the Paramagnetic Range of $(ZrO_2)_{0.9}(Y_2O_3)_{0.08}(Fe_2O_3)_{0.02}$ (I) and $(ZrO_2)_{0.9}(Y_2O_3)_{0.07}(Fe_2O_3)_{0.03}$ (II) Samples after Heat Treatment at 1623 K[a]

sample	ion, phase	IS, mm/s	QS, mm/s	fwhm, mm/s	*S*, %	S_0, %
I′	Fe_1^{3+}	0.60	0.61	0.41	21.4	
	Fe_2^{3+}	0.64	1.16	0.41	57.1	
	Fe_3^{3+}	0.63	1.74	0.42	21.5	
II′	α-Fe_2O_3	0.75	2.55	0.22	5.4	32.4
	Fe_1^{3+}	0.61	0.64	0.41	16.6	11.9
	Fe_2^{3+}	0.64	1.12	0.47	56.6	40.4
	Fe_3^{3+}	0.64	1.67	0.43	21.4	15.3

[a] The notations are the same as in Table 3; S_0 = relative area of component, calculated for six-line hematite spectrum.

different polymorphs: 0.84−0.85 for *m*-ZrO_2, 0.857−0.86 for *t*-ZrO_2, and ≥0.87 for *c*-ZrO_2. For the investigated system $(ZrO_2)_{0.9}(Y_2O_3)_{0.1-x}(Fe_2O_3)_x$ with cubic structure, the average cation radii range between 0.837 and 0.86, which is characteristic of *m*-ZrO_2 and *t*-ZrO_2 but not of *c*-ZrO_2. Along with the steric factor, other factors can affect the stabilization of high-temperature ZrO_2. We consider that in the $ZrO_2-Y_2O_3-Fe_2O_3$ system, the cubic phase can be stabilized by the formation of a compound isomorphic to *c*-ZrO_2.

In the binary system $Y_2O_3-Fe_2O_3$, two phases are formed on the heat treatment of xerogel (hydroxides and alkoxides):[31,32] orhoferrite $YFeO_3$ with distorted perovskite structure and ferrogarnet $Y_3Fe_5O_{12}$. The MS of the $(ZrO_2)_{0.9}(Y_2O_3)_{0.7}$-$(Fe_2O_3)_{0.03}$ sample contains lines of $YFeO_3$ after heat treatment at 1473 K but does not contain them after heat treatment at 1623 K (Figure 4, Table 3). This fact shows that $YFeO_3$ dissolves in *c*-ZrO_2. A few modifications of $YFeO_3$ are known. At 993−1073 K, the $YFeO_3$ phase has a hexagonal unit cell (a = 3.511, c = 11.72, V = 125.12, Z = 2), and at 1153−1203 K,

it has an orthorhombic unit cell ($a = 5.280$, $b = 5.592$, $c = 7.602$, $V = 224.76$, $Z = 4$).[32] At higher temperatures, the unit cell of $YFeO_3$ phase has cubic symmetry.[33] The angle Y−Y−Y in the low-temperature hexagonal unit cell is 60°. It is known[32] that crystal lattice containing face-centered cubic unit cells (of CaF_2 type) can be represented as crystal lattice containing rhombohedra with a sharp angle of 60°. This fact as well as the close unit cell volumes of *c*-ZrO_2 and *h*-$YFeO_3$ allow the statement that these phases are isomorphic. Therefore, the nonequivalent positions of the Fe^{3+} ions (see Table 4) differ in cationic and anionic environment not only in the second, but also in the first coordinating sphere, which is responsible for different local distortions of oxygen octahedrons.

Hexagonal $YFeO_3$ and ZrO_2 can form solid solutions at relatively low temperatures, which are comparable with the *h*-$YFeO_3$ formation temperatures; this facilitates the formation of a wide *c*-ZrO_2 region (Figure 1, Table 1).[10] At 1373−1473 K, *c*-ZrO_2 containing 3 mol % Fe_2O_3 is destabilized (Figure 2), probably due to the segregation of Y^{3+} and Fe^{3+} ions to the grain boundaries.[34] However at 1473 K, this sample is stabilized due to $YFeO_3$ dissolution in the crystal lattice of *c*-ZrO_2. The temperature dependence of *c*-ZrO_2 unit cell parameter supports this statement (Figure 3). In our view, the formation of Y−Fe bonds, which are more covalent than Y−O bonds, prevents Y_2O_3 segregation at the grain boundaries and, consequently, the phase transition of *c*-ZrO_2 → *t*-ZrO_2 → *m*-ZrO_2 type.

The structure of stabilized zirconium dioxide degrades during storage due to *c*-ZrO_2 → *t*-ZrO_2 → *m*-ZrO_2 transition.[35] XRPD investigations showed that the phase composition of $(ZrO_2)_{0.9}(Y_2O_3)_{0.1-x}(Fe_2O_3)_x$ samples remained unchanged after storage in air for 2 years. MS studies showed that the structure of iron-containing SS with tetragonal-distorted fluorite structure is stable in time;[10] in other words, the partial substitution of Fe^{3+} for Y^{3+} contributes to structure stability of high-temperature ZrO_2 in time. In ref 9, the structure degradation of yttrium-stabilized zirconium dioxide is accounted for by martensitic *t*-ZrO_2 → *m*-ZrO_2 transformation, which is activated by water adsorption. The structure of iron-containing high-temperature ZrO_2 is probably stabilized due to the decrease of its hydrophilic property as a consequence of the $YFeO_3$ compound formation.

Conclusion

The effect of iron oxide on the polymorphic composition and fine structure of cubic solid solutions of $(ZrO_2)_{0.9}(Y_2O_3)_{0.1-x}(Fe_2O_3)_x$ system has been investigated. The maximum Fe_2O_3 solubility in the studied cut of a ternary system has been determined to be 2 mol %. Iron exists only as Fe^{3+} ions in octahedral coordination. Three nonequivalent positions of the Fe^{3+} ions, which differ in surrounding cations and anions, have been identified.

It has been shown that the partial substitution of Fe^{3+} ions for Y^{3+} ions increases Y_2O_3 efficiency as a stabilizer of high-temperature ZrO_2 and structure stability in time due to the formation of yttrium orthoferrite ($YFeO_3$), which is isomorphic to *c*-ZrO_2. These results can extend the present-day knowledge of ZrO_2 stabilization mechanism.

References and Notes

(1) Karavaev, Y. N.; Burmakin, E. I. *Inorg. Mater.* **1996**, *32* (1), 66−70.
(2) Matsui, N.; Takigawa, H. *Solid State Ionics* **1990**, *40* (41), 926−928.
(3) Karavaev, Y. N.; Martem'yanova, Z. S.; Zyryanov, V. G. *Inorg. Mater.* **1995**, *31* (7), 937−941.
(4) Shannon, R. D. *Acta Crystallogr. A* **1976**, *32*, 751−767.
(5) Stafford, R. J.; Rothman, S. J.; Routbort, J. L. *Solid State Ionic* **1989**, *37*, 67−72.
(6) Badwal, S. P. S. *Solid State Ionic* **1992**, *52*, 23−32.
(7) Boutz, M. M. R.; Winnubst, A. J. A.; Hartgers, F.; Burggraaf, A. J. *J. Mater. Sci.* **1994**, *29*, 5374−5382.
(8) Shu, J. L.; Yen, T. S.; Schubert, H. *J. Mater. Sci.* **1997**, *32*, 1341−1346.
(9) Alekseenko, V. I.; Volkova, G. K. *J. Tech. Phys.* **2000**, *70* (9), 57−62.
(10) Belous, A. G.; Pashkova, E. V.; V'yunov, O. I.; Ivanitskii, V. P. *J. Mater. Sci.* **2005**, *40*, 5273−5280.
(11) Karavaev, Y. N.; Burmakin, E. I. *Elektrokhimiya* **1992**, *28* (10), 1484−1489.
(12) Scott, H. G. *J. Mater. Sci.* **1975**, *10*, 1527.
(13) Knipovich, Y. N.; Marachevskii, Y. V. *Analysis of mineral raw materials*, 2nd ed.; State Sci.-Tech. Press of Chem. Literature: Leningrad, 1956; p 1055.
(14) Certificate of Analysis. *Standard Reference Material 1976, Instrument Sensitivity Standard for X-ray Powder Diffraction*; National Institute of Standards & Technology: Gaithersburg, MD, 1991.
(15) Yu, Z.; Ting-Chuan, L. *J. Am. Ceram. Soc.* **1991**, *74* (3), 633−640.
(16) Kistner, O. C.; Sunyar, A. W. *Phys. Rev.* **1962**, *125* (4), 1158−1165.
(17) Shirane, G.; Cox, D. E.; Ruby, S. L. *Phys. Rev.* **1962**, *125* (4), 1158−1165.
(18) Eibschutz, M.; Shtrikman, S.; Treves, D. *Phys. Rev.* **1967**, *156* (2), 562−577.
(19) Novikov, G. V. *Method for the analysis of slightly resolved spectra*; deposition VINITI, N4112−B87, 1987.
(20) Bancroft, G. M. F.; Maddoc, A. G.; Burus, R. G. *Geochim. Cosmochim. Acta* **1970**, *37* (1), 2219−2246.
(21) Nasrallah, M. M.; Douglass, D. L. *J. Electrochem. Soc.* **1974**, *121* (2), 255−262.
(22) Olkhovik, G. A.; Naumov, I. I.; Velikokhatnyi, N. N. *Inorg. Mater.* **1993**, *29* (5), 636−640.
(23) Berry, F. I.; Loretto, M. H.; Smith, M. R. *J. Solid State Chem.* **1989**, *83* (1), 91−99.
(24) Tikhonov, F. N.; Archenin, V. Ya. *Methods of solving of incorrect problems*; Nayka: Moscow, 1979.
(25) Rusakov, V. S. *Izv. RAN. Ser. Fiz.* **1999**, *6* (7), 1389−1390.
(26) Zyuzin, D. A.; Moroz, E. M.; Ivanova, A. S.; Zajkovskii, V. I. *Inorg. Mater.* **2000**, *36* (4), 447−451.
(27) Neuimin, A. D.; Kotlyar, A. G.; Palguev, S. F.; Strekalovskii, V. N.; Batrakov, N. A. *Proc. Inst. Electrochem. UF AN USSR* **1969**, *12*, 92−112.
(28) Belous, A. G.; Pashkova, E. V.; Makarenko, A. N.; Khomenko, B. S. *Inorg. Mater.* **1997**, *33* (1), 52−55.
(29) Matsuiv, N.; Takigawa, M. *Solid State Ionics*, **1990**, *40* (41), 926−928.
(30) Strelkov, K. K.; Sumin, V. I.; Pliner, S. Y. *Self-propagating high temperature synthesis. Transformation hardening of refractory materials*; Sverdlovsk, 1989.
(31) Lukachina, E. P.; Stetsenko, V. I.; Yermolenko, I. V. *Inorg. Mater.* **1977**, *14*(1), 102−105.
(32) Yamagudii, Q.; Takimura, H.; Yamashita, M. *J. Electochem. Soc.* **1991**, *138*, 1492.
(33) Keth, M. L.; Roy, R. *Am. Miner.* **1954**, *39*, 1.
(34) Bokij, T. B. *Crystal chemistry*; Nauka: Moscow, 1971.
(35) Belous, A. G.; Makarenko, A. N.; Pashkova, E. V.; Khomenko, B. S. *Inorg. Mater.* **1999**, *35*(11), 1341−1343.